The $Cr^{II}L$ Reduction of [2Fe-2S] Ferredoxins and Site of Attachment of Cr^{III} Using ^1H NMR and Site-Directed Mutagenesis

S.-C. Im,[†] J. A. R. Worrall,[†] G. Liu,[‡,§] A. Aliverti,[||] G. Zanetti,[||] C. Luchinat,[‡,⊥] I. Bertini,[‡,§] and A. G. Sykes*[,†]

Department of Chemistry, The University of Newcastle, Newcastle upon Tyne, NE1 7RU, U.K., Magnetic Resonance Centre, University of Florence, Via L. Sacconi 6, 50019 Sesto Fiorentino, Italy, Department of Chemistry, University of Florence, Via G. Capponi 7, 50121 Florence, Italy, Department of General Physiology and Biochemistry, University of Milan, Via Celoria 26, 20133 Milan, Italy, and Department of Soil Science and Plant Nutrition, University of Florence, P. delle Cascine 28, 50144 Florence, Italy

Received September 21, 1999

The recently reported NMR solution structure of $Fe^{III}Fe^{III}$ parsley FdI has made possible 2D NOESY NMR studies to determine the point of attachment of $Cr^{III}L$ in $Fe^{III}Fe^{III}$...$Cr^{III}L$. The latter Cr-modified product was obtained by reduction of $Fe^{III}Fe^{III}$ parsley and spinach FdI forms with $[Cr(15\text{-ane}N_4)(H_2O)_2]^{2+}$ (15-aneN_4 = 1,4,8,12-tetraazacyclopentadecane), referred to here as $Cr^{II}L$, followed by air oxidation and chromatographic purification. From a comparison of NMR cross-peak intensities of native and Cr-modified proteins, two surface sites designated A and B, giving large paramagnetic $Cr^{III}L$ broadening of a number of amino acid peaks, have been identified. The effects at site A (residues 19−22, 27, and 30) are greater than those at site B (residues 92−94 and 96), which is on the opposite side of the protein. From metal (ICP-AES) and electrospray ionization mass spectrometry (EIMS) analyses on the Cr-modified protein, attachment of a single $Cr^{III}L$ only is confirmed for both parsley and spinach FdI and FdII proteins. Electrostatic interaction of the 3+ $Cr^{III}L$ center covalently attached to one protein molecule (charge ∼−18) with a second (like) molecule provides an explanation for the involvement of two regions. Thus for 3−4 mM $Fe^{III}Fe^{III}$...$Cr^{III}L$ solutions used in NMR studies ($Cr^{III}L$ attached at A), broadening effects due to electrostatic interactions at B on a second molecule are observed. Experiments with the Cys18Ala spinach FdI variant have confirmed that the previously suggested Cys-18 at site A is not the site of $Cr^{III}L$ attachment. Line broadening at Val-22 of A gives the largest effect, and $Cr^{III}L$ attachment at one or more adjacent (conserved) acidic residues in this region is indicated. The ability of $Cr^{II}L$ to bind in some (parsley and spinach) but not all cases (*Anabaena variabilis*) suggests that intramolecular H-bonding of acidic residues at A is relevant. The parsley and spinach $Fe^{II}Fe^{III}$...$Cr^{III}L$ products undergo a second stage of reduction with the formation of $Fe^{II}Fe^{II}$...$Cr^{III}L$. However, the spinach Glu92Ala (site B) variant undergoes only the first stage of reduction, and it appears that Glu-92 is required for the second stage of reduction to occur. A sample of $Cr^{III}L$-modified parsley $Fe^{III}Fe^{III}$ Fd is fully active as an electron carrier in the NADPH−cytochrome *c* reductase reaction catalyzed by ferredoxin−$NADP^+$ reductase.

Introduction

The [2Fe-2S] ferredoxins (Fd) function as electron-transfer mediators in many biological processes including photosynthesis, respiration, biosynthesis, and degradative metabolic processes.[1−3] The most extensively studied class is the photosynthetic ferredoxins from plant chloroplasts and cyanobacteria (blue-green algae), the prime function of which is to promote electron transfer (ET) between reduced photosystem I and the enzyme ferredoxin−$NADP^+$ reductase (FNR).[4,5] Amino acid sequencesof [2Fe-2S] ferredoxins from over 75 species have been reported and show considerable homology, with 18 positions totally invariant.[6]

X-ray crystal structures of the protein in the $Fe^{III}Fe^{III}$ state from the blue-green algae *Spirulina plantensis*,[7] *Anabaena* 7120,[8] *Aphanothece sacrum*,[9] and *Halobacterium maris-mortui*[10] and from the plant sources *Equisetum arvense*[11] and *Spinacia oleracea*,[12] and NMR solution structures of proteins also in the

* Correspondence to Professor A. G. Sykes. Tel: 44-191-2226700. E-mail: a.g.sykes@newcastle.ac.uk. Fax: 44-191-2611182.
[†] The University of Newcastle.
[‡] Magnetic Resonance Centre, University of Florence.
[§] Department of Chemistry, University of Florence.
[||] University of Milan.
[⊥] Department of Soil Science and Plant Nutrition, University of Florence.

(1) Arnon, D. I. *Trends Biochem. Sci*. **1988**, *13*, 30−33.
(2) Crawford, N. A.; Yee, B. C.; Droux, M.; Carwon, D. E.; Buckanan, B. B. In *Methods in Enzymology*; Packer, L., Glazer, A. N., Eds.; Academic Press: San Diego, CA, 1988; Vol. 167, p 415.
(3) Schmidt, H.; Heinz, E. *Plant Physiol*. **1990**, *94*, 214−220.
(4) Matsubara, H.; Saeki, K. *Adv. Inorg. Chem*. **1992**, *38*, 223−280.
(5) Cammack, R. *Adv. Inorg. Chem*. **1992**, *38*, 281−322.
(6) Matsubara, H.; Hase, T. In *Proteins and Nucleic Acids in Plant Systematics*; Jensen, H., Fairbrothers D. E., Eds.; Springer-Verlag: New York, 1983.
(7) Tsukihara, T.; Fukuyama, K.; Nakamura, M.; Katsube, T.; Tanaka, N.; Kakudo, M.; Wada, K.; Hase, T.; Matsubara, H. *J. Biochem. (Tokyo)* **1981**, *90*, 1763−1773.
(8) Rypniewski, W. R.; Brieter, D. R.; Benning, M. M.; Wesenberg, G.; Oh, B.-H.; Markley, J. L.; Rayment, I.; Holden, H. M. *Biochemistry* **1991**, *30*, 4126−4131.
(9) Tsukihara, T.; Fukuyama, K.; Mizushima, M.; Harioka, T.; Kusunoki, M.; Katsube, Y.; Hase, T.; Matsubara, H. *J. Biochem*. **1991**, *216*, 399−410.
(10) Sussman, J. L.; Shoham, M.; Harel, M.; Yonath, A. *Acta Crystallogr*. **1984**, *40*, C40.

10.1021/ic991127w CCC: $19.00
Published on Web 03/25/2000

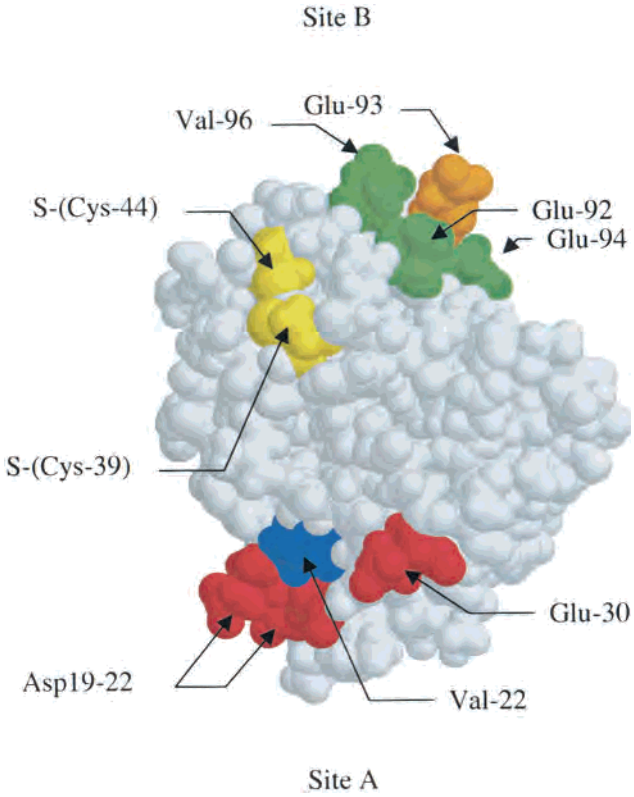

Figure 1. Space-filling representation of the structure of parsley [2Fe-2S] FdI in the $Fe^{III}Fe^{III}$ oxidation state,[16] showing the position of the cysteine ligands (yellow) at the 2Fe site. Amino acids at sites A (red) and B (green), as defined in this work, are indicated. The blue at site A indicates a larger broadening effect, and the orange at B less broadening (see Results).

$Fe^{III}Fe^{III}$ state from *Pseudomonas putida*,[13] *Synechocystis* sp. PCC 6803,[14] *Synechococcus elongatus*,[15] and parsley FdI[16] have been reported. A space-filling structure of parsley FdI, with the positions of amino acids relevant to this study, is shown in Figure 1.

Photosynthetic ferredoxins ($M_r \sim 10.5$ kDa; 93−99 amino acids) contain a single [2Fe-2S] cluster and have two high-spin tetrahedral Fe^{III} atoms ($S = {}^5/_2$) bridged by two μ-sulfido ligands, which are antiferromagnetically coupled and therefore EPR silent.[17] The binuclear Fe core is coordinated to four cysteines at positions 39, 44, 47, and 77, in the polypeptide chain (numbering as in ref 16). One-electron-reduction potentials (vs NHE) for higher plant $Fe^{III}Fe^{III}$ ferredoxins are in the range -430 ± 20 mV,[18] and for cyanobacteria ferredoxins are in the range −310 to −380 mV.[19] The [2Fe-2S] ferredoxins are very acidic, with p*I* values from 3 to 4. From the amino acid

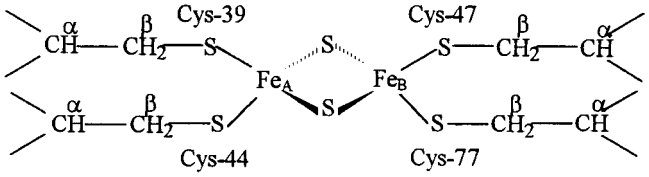

Figure 2. Active site of [2Fe-2S] ferredoxins, with Fe_A (close to the surface) and Fe_B defined as in ref 20.

composition, taking account of the charge on residues Glu/Asp (1−), Arg/Lys (1+), and the active site, the charge balance for the $Fe^{III}Fe^{III}$ proteins is −18 (±2) at pH 7.5. One of the metal atoms, Fe_A, is close to the surface (∼5 Å), and the Cys-39 and Cys-44 residues bound to it are partially exposed to solvent water. Although there is no crystal structure for the $Fe^{II}Fe^{III}$ state, it has been shown by NMR that the extra electron is localized on Fe_A with Fe_B assigned as Fe^{III} [20] (Figure 2). An X-ray structure of the $Fe^{II}Fe^{III}$ protein from *Anabaena* PCC 7119 has recently been reported at 1.17 Å (Morales, R.; Chron, M. H.; HudryClergeon, G.; Petillot, Y.; Norager, S.; Medina, M.; Frey, M. *Biochemistry* **1999**, *38*, 15764−15773). The [2Fe-2S] ferredoxins as isolated have two different molecular components.[6] Such isoferredoxins can be separated by Phenyl Superose HR5/5 hydrophobic column chromatography, with FdI the major and FdII the minor component. In the case of spinach the two forms have the same charge, but 24 amino acids are different[21] (Figure 3). Furthermore, spinach FdI has been cloned and overexpressed in *Escherichia coli*.

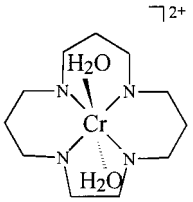

The reduction of parsley and spinach FdI forms with the 1,4,8,12-tetraazacyclopentadecane complex $[Cr(15\text{-ane}N_4)(H_2O)_2]^{2+}$, abbreviated $Cr^{II}L$, has provided the first evidence for a 2 equiv reduction of $Fe^{III}Fe^{III}$ ferredoxins to the $Fe^{II}Fe^{II}$ state.[22] The $Cr^{III}L/Cr^{II}L$ couple has a reduction potential of −580 mV (vs NHE) at $[H^+] = 0.4$ M.[23] An important feature of the double reduction is the covalent attachment of $Cr^{III}L$ to the $Fe^{II}Fe^{III}$ formed in the first step, which perturbs the protein sufficiently to make the second reduction possible (Scheme 1).

Information regarding the point of attachment of $Cr^{III}L$ is important because of the unexpected influence it has on reactivity, making it possible to further reduce the $Fe^{II}Fe^{III}$ protein to $Fe^{II}Fe^{II}$. Mössbauer evidence for the $Fe^{II}Fe^{II}...Cr^{III}L$ state has recently been reported in a ferredoxin from *Aquifex aeolicus* (Yoo, S. J.; Meyer, J.; Münck, E. *J. Am. Chem. Soc.* **1999**, *121*, 10450−10451). In view of the substitution inertness of $Cr^{III}L$, the point of attachment also defines the distance for electron transfer from the $Cr^{II}L$ reductant to the $Fe^{III}Fe^{III}$ active site. From studies on spinach and parsley FdI ($Cr^{III}L$ attached) and *Anabaena variabilis* FdI (no $Cr^{III}L$ attached), a correlation of attachment with the presence of an uncoordinated cysteine at position 18 has been noted (Figure 3), and Cys-18 was

(11) Ikemitzu, S.; Bando, M.; Sato, T.; Morimoto, Y.; Tsukihara, T. *Acta Crystallogr.* **1994**, *50D*, 167−174.
(12) Binda, C.; Coda, A.; Aliverti, A.; Zanetti, G.; Mattevi, A. *Acta Crystallogr., Sect. D* **1998**, *54D*, 1353−1358.
(13) Pochapsky, T. C.; Mei Ye, X.; Ratnaswamy, G.; Lyons, T. A. *Biochemistry* **1994**, *33*, 6424−6432.
(14) Lelong, C.; Sétif, P.; Bottin, H.; André, F.; Neumann, J.-M. *Biochemistry* **1995**, *34*, 14462−14473.
(15) Baumann, B.; Sticht, H.; Schärpf, M.; Sutter, M.; Haehnel, W.; Rösch, P. *Biochemistry* **1996**, *35*, 12831−12841.
(16) Im, S.-C.; Liu, G.; Luchinat, C.; Sykes, A. G.; Bertini, I. *Eur. J. Biochem.* **1998**, *258*, 465−477.
(17) Nakano, T.; Hase, T.; Matsubara, H. *J. Biochem.* **1981**, *90*, 1725−1730.
(18) Salamon, Z.; Tollin, G. *Bioelectrochem. Bioenerg.* **1992**, *27*, 381−391.
(19) Cammack, R.; Rao, K. K.; Bargeron, C. P.; Hutson, K. G.; Andrews, P. W.; Rogers, L. J. *J. Biochem.* **1977**, *168*, 205−209.
(20) Dugad, L. B.; MaMar, G. N.; Banci, L.; Bertini, I. *Biochemistry* **1990**, *29*, 2263−2271.
(21) Takahashi, Y.; Hase, T.; Wada, K.; Matsubara, H. *Plant Cell Physiol.* **1983**, *24*, 189−198.
(22) Im, S.-C.; Lam, K.-Y.; Lim, M.-C.; Ooi, B.-L.; Sykes, A. G. *J. Am. Chem. Soc.* **1995**, *117*, 3635−3636.
(23) Sammuels, G. J.; Espenson, J. H. *Inorg. Chem.* **1979**, *18*, 2587−2592.

```
                    10          20          30          40          50
                                                        *     *  *
(a) AA YKVTLVT-PT  G-NVEFQCPD  DVYILDAAEE  EGIDLPYSCR  AGSCSSCAGK
(b) AT YKVTLVT-PS  G-SQVIECGD  DEYILDAAEE  KGMDLPYSCR  AGACSSCAGK
(c) AT YNVKLIT-PD  G-EVEFKCDD  DVYVLDQAEE  EGIDIPYSCR  AGSCSSCAGK
(d) AT FKVKLINEAE  GTKHEIEVPD  DEYILDAAEE  QGYDLPFSCR  AGACSTCAGK

            60          70          80          90
                                    *
(a) LKTGSLNQDD  QSFLDDDQID  EGWVLTCAAY  PVSDVTIETH  KEEELTA
(b) VTSGSVDQSD  QSFLEDGQME  EGWVLTCIAY  PTGDVTIETH  KEEELTA
(c) VVSGSIDQSD  QSFLDDEQMD  AGYVLTCHAY  PTSDVVIETH  KEEEIV
(d) LVSGTVDQSD  QSFLDDDQIE  AGYVLTCVAY  PTSDVVIQTH  KEEDLY
```

Figure 3. Amino acid sequences for [2Fe-2S] Fds relevant to this study: (a) spinach FdI,[4] (b) spinach FdII,[4] (c) parsley FdI[6] (that of FdII not yet determined), and (d) *A. variabilis* FdI.[4]

Scheme 1

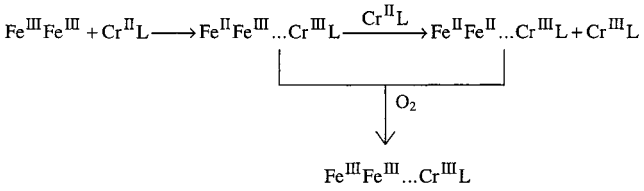

suggested as a possible point of $Cr^{III}L$ attachment.[24] With information provided by the NMR solution structure of $Fe^{III}Fe^{III}$ parsley FdI,[16] and knowledge that Cr^{III} has a slow electronic relaxation time ($t = 5 \times 10^{-9}$s) which causes dramatic NMR line broadening,[24] NMR line-broadening effects are now examined in more detail, and hence the point of attachment of $Cr^{III}L$ in $Fe^{III}Fe^{III}$...$Cr^{III}L$ is determined.

Experimental Section

Isolation and Purification of [2Fe-2S] Ferredoxins. The [2Fe-2S] ferredoxins from fresh parsley and spinach leaves were isolated by standard literature methods.[26,27] Samples of [2Fe-2S] Fds were stored as the $Fe^{III}Fe^{III}$ protein at −80 °C under N_2. The purity was checked using ratios of UV−vis absorbance at 422 and 278 nm. Ratios A_{422}/A_{278} (FdI and FdII) obtained for spinach >0.46 (in this work 0.48) and for parsley >0.60 (0.63) were used.

Separation of FdI and FdII Components. A Phenyl Superose HR5/5 hydrophobic column attached to a Pharmacia FPLC (fast protein liquid chromatography) system was used.[28] All buffers were deoxygenated by bubbling N_2 through solutions to minimize the loss of Fd. The buffers used for separation were buffer A, 20 mM Tris/HCl, pH 7.5, and buffer B, 20 mM Tris/HCl, pH 7.5 containing 1.7 M ammonium sulfate. The column was equilibrated in buffer B, and the protein was filtered and loaded onto the column in the same buffer. Separation was achieved using a linear gradient (1.75% per cm^3) of 0−50% A with a flow rate of 0.5 cm^3 min^{-1}. Elution was monitored at 280 nm using a UV-M control. The purified iso forms were exchanged into 20 mM Tris/HCl, pH 7.5, I = 0.100 M (NaCl) using an Amicon cell fitted with a YM3 membrane.

Preparation of Spinach FdI Variants. Recombinant spinach ferredoxin I variants were prepared in the Department of General Physiology and Biochemistry at the University of Milan. The Glu92Ala variant was obtained by site-directed mutagenesis, where the purification and biochemical characterization were as previously described.[29] The Cys18Ala variant was obtained for the present work using the Quick Change site-directed mutagenesis kit by Stratagene, with pETFdI[30] as template. The presence of the desired mutation and lack of second site mutations were confirmed by sequencing the entire ferredoxin gene. The Cys18Ala ferredoxin I was purified using the same procedure described for purification of the wild-type recombinant ferredoxin I.[30] The variant displayed an absorption spectrum similar to that of the wild-type protein. Its electron-transfer properties were comparable to those of the wild-type ferredoxin I in the NADPH−cytochrome *c* reaction, using spinach ferredoxin−$NADP^+$ reductase as catalyst. Further biochemical characterization of the Cys18Ala variant will be reported elsewhere. Samples of Glu92Ala and Cys18Ala spinach ferredoxin I used throughout this work were homogeneous, based on electrophoresis and absorbance ratios A_{422}/A_{278} >0.48.

Buffer Solutions. Solutions of tris(hydroxymethyl)methylamine (pK_a = 8.08) were used in kinetic studies, here referred to as Tris, with 1.0 M HCl (Convol) added to give pH's in the range 7.0−8.9 as required. For electrospray ionization mass spectrometry (EIMS) ammonium acetate buffer (pK_a = 4.76) was used, and the pH, was adjusted with 1.0 M NaOH (Convol). For NMR solutions sodium hydrogen phosphate buffer (pK_a = 6.68) was used. All buffers were obtained from Sigma and were adjusted to I = 0.100 M with NaCl (BDH, Analar). A Radiometer PHM62 pH meter, complete with a Russell CWR/320/757 pH electrode or, for measurement in an NMR tube, a narrow Russell CMAWL/3.7/180 pH electrode, was used to measure the pH.

Other Reagents. Sodium dithionite, $Na_2S_2O_4$ (Sigma Chemicals 86%), was standardized spectrophotometrically by addition of an excess of $[Fe(CN)_6]^{3-}$ (Aldrich 99%), followed by determination of unreacted complex at 420 nm (ϵ = 1010 M^{-1} cm^{-1}). Deuterium oxide (Goss Scientific Instruments Ltd; 99.9% D min) was used for the preparation of NMR samples.

Preparation of the $[Cr(15\text{-ane}N_4)(H_2O)_2]^{2+}$ Complex. A sample of chromium(II) chloride, $CrCl_2 \cdot 4H_2O$, was prepared by a literature method.[31] Required amounts of the ligand 1,4,8,12-tetraazacyclopentadecane (Strem Chemicals), 15-aneN_4, were added to $CrCl_2 \cdot 4H_2O$ in deoxygenated 20 mM Tris/HCl, pH 7.5 to give $[Cr(15\text{-ane}N_4)(H_2O)_2]^{2+}$, I = 0.100 M (NaCl). The latter is likely to be the trans isomer by analogy with *trans*-$[Cr(15\text{-ane}N_4)(H_2O)(NCS)]^{2+}$.[32] Rigorous air-free techniques were employed using a glovebox (O_2 < 3 ppm). The UV−vis absorbance peak λ/nm (ϵ/M^{-1} cm^{-1}) for $Cr^{II}L$ over a wide range of

(24) Im, S.-C.; Kohzuma, T.; McFarlane, W.; Galliard, J.; Sykes, A. G. *Inorg. Chem.* **1997**, *36*, 1388−1396.
(25) DeBoer, E.; VanWilligen, H. *Prog. Nucl. Magn. Reson. Spectrosc.* **1967**, *2*, 111.
(26) Plesnicar, M.; Bendall, D. S. *Biochim. Biophys. Acta* **1970**, *216*, 192−199.
(27) Ellefson, W. A.; Ulrich, E. A.; Krogmann, D. W. *Methods Enzymol.* **1980**, *69*, 223−228.
(28) Sakihama, N.; Shin, M.; Toda, H. *J. Biochem.* **1986**, *100*, 43−47.
(29) Piubelli, L.; Aliverti, A.; Bellintani, F.; Zanetti, G. *Eur. J. Biochem.* **1996**, *236*, 465−469.
(30) Piubelli, L.; Aliverti, A.; Bellintani, F.; Zanetti, G. *Protein Expression Purif.* **1997**, *1342*, 298−304.
(31) Holah, D. G.; Fackler, J. P. *Inorg. Synth.* **1969**, *10*, 26−35.
(32) Clegg, W.; Leupin, P.; Richens, D. T.; Sykes, A. G.; Roper, E. S. *Acta Crystallogr.* **1985**, *C41*, 530−532.

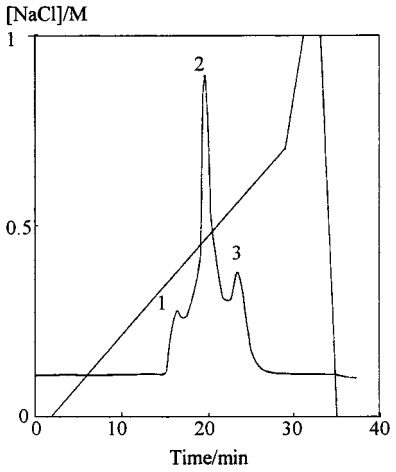

Figure 4. Illustration of FPLC Mono-Q separation of components of a $Cr^{III}L$-modified sample containing parsley $Cr^{III}L$-modified Fe^{III}-Fe^{III}...$Cr^{III}L$ protein using buffers A (20 mM Tris/HCl at pH 7.5) and B (20 mM Tris/HCl at pH 7.5 in 1.0 M NaCl) as gradient. The flow rate was 0.5 cm^3/min^{-1}, with the absorbance peak selected at 280 nm. The peak labeled 1 gave no color and no Fe or Cr content; peak 2 was assigned to $Cr^{III}L$-modified; and peak 3 to native FdI protein.

pH's (5.0−9.0) is at 540 (ϵ = 36.5).[33] Upon air oxidation the $Cr^{III}L$ product $[Cr(15\text{-ane}N_4)H_2O)_2]^{3+}$ is formed; at pH 1.5 it has peak positions 337 (88) and 454 (87) as previously reported.[33] The Cr^{III} complex has pK_a (25 °C) values of 2.9 and 7.8, and pH's <7.5 were therefore chosen for the present studies.[33] As far as $Cr^{II}L$ is concerned the two axial H_2O's will be kinetically very labile,[34] whereas with $Cr^{III}L$ all ligands are inert.

Preparation of the $Fe^{III}Fe^{III}$...$Cr^{III}L$ Form. For parsley and spinach FdI addition of a 3-fold excess of Cr^{II} L to the $Fe^{III}Fe^{III}$ protein at pH 7.5 (20 mM Tris/HCl), I = 0.100 M (NaCl), was carried out in the glovebox. This was followed by rapid air oxidation, DE-52 column separation of excess $Cr^{III}L$, and separation of products by Mono-Q Pharmacia FPLC anion-exchange column chromatography, to give the Fe^{III} Fe^{III}...$Cr^{III}L$ product as previously described.[24] The FPLC elution profiles for solutions following $Cr^{II}L$ reduction of parsley and spinach FdI are different from those for native Fd (single band). Three bands were observed (Figure 4). The first had no color and no Fe or Cr content. The second having by far the greatest intensity analyzed for Cr-modified protein, and the third was a small amount of unreacted native Fd. The same procedures were used for parsley and spinach FdII and variant forms. Both FdII forms were found to undergo 2 equiv reduction with excess $Cr^{II}L$ as in Scheme 1. The $Cr^{III}L$-modified products are stable at 25 °C under anaerobic conditions. Reactions of the two variant forms with $Cr^{II}L$ are considered in Results.

Metal Analyses of $Fe^{III}Fe^{III}$...$Cr^{III}L$ Products. These were carried out by inductively coupled plasma atomic emission spectroscopy (ICP-AES) and gave Fe:Cr ratios close to 2.0:1.0 (Table 1).

Electrospray Ionization Mass Spectrometry (EIMS). Mass analyses of native and $Cr^{III}L$-modified $Fe^{III}Fe^{III}$ samples were carried out on a Micromass Autospec M triple-focusing magnetic sector instrument. Samples were prepared in 10 mM ammonium acetate pH 7.28 with the concentration of protein ~400 mM. The samples were run in the negative detection mode so as to preserve the iron−sulfur cluster.[35] The infusion solvent for the negative detection mode (which is taken up by the instrument after the Fd sample) was 60:40 acetonitrile and water, pH 8.6. For Cr-modified parsley and spinach the EIMS data gave M_r's of 10958.4 ± 1 and 10954.2 ± 1 Da, respectively, with the M_r of the two native Fds given in Table 1, in good agreement with reported values.[35] The M_r of the $Cr^{II}L$ macrocyclic complex is 302 Da, where it is assumed that covalent attachment of $Cr^{III}L$ to the protein results in the loss of an axial water molecule to give a unit of 284 Da. From mass analysis data, Table 1, both parsley and spinach FdI conform with AES-ICP analyses in that only one $Cr^{III}L$ is attached. The results indicate additional 13 Da (parsley) and 10 Da (spinach) contributions to formula weights of the Cr-modified proteins, Table 1. Such discrepancies are attributed to different degrees of protonation under the conditions employed.

Table 1. Inductively Coupled Plasma Atomic Emission Spectroscopy (ICP-AES) and Electrospray Ionization Mass Spectrometry (EIMS) Analyses of [2Fe-2S] FdI and FdII Iso Forms and $Cr^{III}L$-Modified Proteins

source	protein	Fe:Cr	M_r/Da
parsley FdI	$Fe^{III}Fe^{III}$		10661.6(1)
	$Fe^{III}Fe^{III}$...$Cr^{III}L$	2.0:0.9	10958.4(2)[a,b]
parsley FdII	$Fe^{III}Fe^{III}$		
	$Fe^{III}Fe^{III}$...$Cr^{III}L$	2.0:1.17	
spinach FdI	$Fe^{III}Fe^{III}$		10660.3(1)[f]
	$Fe^{III}Fe^{III}$...$Cr^{III}L$	2.0:1.0	10954.2(1)[a,c]
spinach FdII	$Fe^{III}Fe^{III}$		10507.9(1)
	$Fe^{III}Fe^{III}$...$Cr^{III}L$	2.0:1.0	
spinach Cys18Ala	$Fe^{III}Fe^{III}$		10625.2(1)
	$Fe^{III}Fe^{III}$...$Cr^{III}L$	2.0:1.1	10916.3(3)[a,b]
spinach Glu92Ala	$Fe^{III}Fe^{III}$		10597.0(1)
	$Fe^{III}Fe^{III}$...$Cr^{III}L$	2.0:1.2	10900.4(2)[a,e]

[a] To be compared with the calculated value assuming covalent attachment of $Cr(15\text{-ane}N_4)H_2O^{3+}$ to the proteins,which gives [b](10945.6), [c](10944.3), [d](10909.2), and [e](10882.0), respectively. [f] For other published values, see ref 35.

NMR Spectroscopy. Samples of native and Cr-modified (Fe^{III}-Fe^{III}...$Cr^{III}L$) parsley FdI, pH 7.5 (46 mM sodium phosphate), I = 0.100 M (NaCl), were prepared in H_2O/D_2O (90:10) solution, using ultrafiltration methods (Amicon; YM3 membrane). Concentrations of native and Cr-modified protein were determined by UV−vis spectrometry at 422 nm (ϵ = 9200 M^{-1} cm^{-1}). Protein concentrations used were 3.0−4.0 mM. The protein solution was loaded into an NMR tube, previously flushed with argon, and sealed. All ^1H NMR spectra for this study were acquired at 200.13, 600.13, and 800.13 MHz on MSL200, AMX600, and AVANCE 800 Bruker spectrometers. The 1D ^1H NMR spectra were recorded using the super WEFT (water-eliminated Fourier transform) pulse sequence,[36] with a recycle delay range from 200 ms to 1s. The spectra were taken at 288, 298, and 303 K, using presaturation or watergate during relaxation delay and mixing time.[37] Two-dimensional TPPI NOESY spectra were acquired at 298 K, using a spectral width of 13−14 ppm, with a recycle time of 1 s and mixing times of 40, 100, and 300 ms.[38,39] All 2D spectra consisted of 4K data points in the F2 dimension and 512 increments in the F1 dimension, using 112 scans per experiment. Raw data were multiplied in both dimensions by a pure cosine-squared and Fourier transformed to obtain 1024 × 1024 real data points with a polynomial baseline correction applied in both directions. All the spectra were calibrated from the chemical shifts 4.93, 4.81, and 4.77 ppm of the water signal at 288, 298, and 303 K, respectively. All NMR data were processed with the Bruker UXNMR and XWINNMR software packages. The program XEASY (ETH Zürich) was used for analyses of the 2D spectra.[40]

Kinetic Studies. An Applied Photophysics SX-17MV stopped-flow reaction analyzer was used to monitor absorbance decay at the 422 nm $Fe^{III}Fe^{III}$ Fd peak, which gives $\Delta\epsilon$ = 4500 M^{-1} cm^{-1} for the first stage of reduction to $Fe^{II}Fe^{III}$.[41] The further decrease in absorbance for the second stage of reduction to $Fe^{II}Fe^{II}$ (when effective) was monitored

(33) Richens, D. T.; Adzamali, I. K.; Leupin, P.; Sykes, A. G. *Inorg. Chem.* **1984**, *23*, 3065−3069.
(34) Lincoln, S. F.; Merbach, A. E. *Adv. Inorg. Chem.* **1995**, *42*, 1−88.
(35) Petillot, Y.; Forest, E.; Meyer, J.; Moulis, J.-M. *Anal. Biochem.* **1995**, *228*, 56−63.
(36) Banci, L.; Bertini, I.; Luchinat, C.; Piccioli, M.; Scozzafava, A.; Torano, P. *Inorg. Chem.* **1989**, *28*, 4650−4656.
(37) Piotto, M.; Saudek, V.; Skelenar, V. *J. Biomol. NMR* **1992**, *2*, 661−666.
(38) Macura, S.; Wüthrich, K.; Ernst, R. R. *J. Magn. Reson.* **1982**, *47*, 351−357.
(39) Marion, D.; Wüthrich, K. *Biochem. Biophys. Res. Commun.* **1983**, *113*, 967−974.
(40) Eccles, C.; Günter, P.; Billeter, M.; Wüthrich, K. *J. Biomol. NMR* **1981**, *1*, 111−130.
(41) Fee, J. A.; Palmer, G. *Biochim. Biophys. Acta* **1971**, *245*, 175−195.

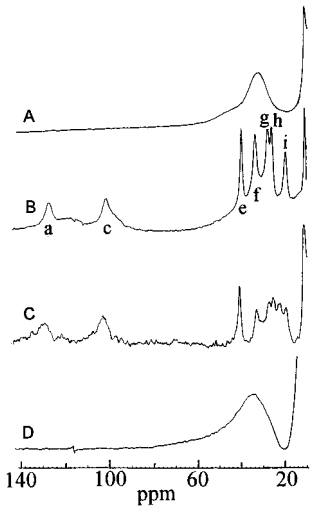

Figure 5. ^{1}H NMR spectra (200 MHz) of parsley FdI forms at 25 °C: (A) native $Fe^{III}Fe^{III}$, (B) native $Fe^{II}Fe^{III}$, (C) $Fe^{II}Fe^{III}$...$Cr^{III}L$, and (D) $Fe^{II}Fe^{II}$...$Cr^{III}L$ at pH 7.5 (46 mM phosphate), $I = 0.100$ M (NaCl).

at the same wavelength ($\Delta\epsilon = 2200$ M^{-1} cm^{-1}). UV−vis contributions from $Cr^{II}L$ or $Cr^{III}L$ are negligible.[33] All reactions were at 25.0 ± 0.1 °C, with 20 mM buffer, and the ionic strength was adjusted to 0.100 ± 0.001 M with NaCl. Concentrations of $Fe^{III}Fe^{III}$Fd used were ~1.0 × 10^{-5} M with the $Cr^{II}L$ in >10-fold excess. An Applied Photophysics software package was used to determine first-order rate constants. Rate constants listed are the mean of absorbance vs time fits for at least five different traces using the same reactant solutions.

Electrochemistry. Square-wave voltammetry measurements on the two spinach FdI variants were carried out as previously reported.[24] A peak at −450 mV vs NHE was obtained for the Cys18Ala variant, and a peak at −342 mV vs NHE for the Glu92Ala variant, in good agreement with a previous value.[42]

Structure Analysis. The programs MOL-MOL and RASMOL[43] were used for solvent accessibility, H-bonding, and structure display calculations.

Results

1D ^{1}H NMR Spectra of Native and Cr-Modified Parsley FdI. The 1D NMR spectra of native and Cr-modified parsley FdI ($Fe^{III}Fe^{III}$...$Cr^{III}L$) were determined at different temperatures (288, 298, 303 K) on a 200 MHz spectrometer. Analyses of 1D ^{1}H NMR for $Fe^{II}Fe^{III}$...$Cr^{III}L$ samples are based on the assumption that the protons of cysteines bound to the Fe^{II} are hyperfine coupled to that metal, and likewise for cysteines bound to the Fe^{III}, Figure 2.[44] The spin of Fe^{III} ($S = {}^5/_2$) will be oriented along the external magnetic field because it is the larger spin, and associated protons will experience contact shifts that decrease with increasing temperature (the Curie effect). The spin of Fe^{II} ($S = 2$) will be oriented in the opposite direction because of the antiferromagnetic coupling to give a total spin of $S' = {}^1/_2$, and associated protons will have less downfield contact shifts that increase with increasing temperature (anti-Curie effect). Spectra of both native and Cr-modified $Fe^{III}Fe^{III}$ forms ($S = 0$) exhibit a broad peak at 34−37 ppm, Figure 5A. This corresponds to the four β-CH_2 protons of the four coordinated cysteines, Figure 2, and a strong anti-Curie temperature dependence is displayed. Spectra of one-electron-reduced samples were obtained by addition of 1 equiv (small excess) of sodium dithionite, Figure 5B,C. The $Fe^{II}Fe^{III}$ components of both native and Cr-modified parsley FdI exhibit the same behavior as previously described for spinach [2Fe-2S] FdI.[45] The peaks at 90−140 ppm (Figure 5B, a and c) show a Curie-type temperature dependence (Figure 6) and are assigned to the two β-CH_2's of the cysteines coordinated to the Fe^{III}. The shoulders in the region are assigned to the other two β-CH_2's. The peak at 43 ppm (e) also exhibits a Curie-type temperature dependence (Figure 6), assigned to the α-CH's of the same cysteines. A set of four signals were observed at 20−35 ppm (f−i), showing an anti-Curie temperature dependence (Figure 6), and are assigned to the four β-CH_2 protons of the cysteines coordinated to the Fe^{II}. A peak at 15 ppm showed little temperature dependence and can be tentatively assigned to the α-CH's of the cysteines attached to the Fe^{II}. A new peak was observed at 25 ppm (288 K) for the one-electron-reduced Cr-modified protein (Figure 5C). Upon addition of an excess (5 equiv) of sodium dithionite, the Cr-modified protein is reduced to the $Fe^{II}Fe^{II}$ state[24] and a broad peak at 34 ppm (Figure 5D) is observed. This is the first 1D spectrum of the $Fe^{II}Fe^{II}$ oxidation state of a [2Fe-2S] Fd determined by NMR. The fully reduced protein was air oxidized after completion of the experiment, with 80% recovery of the $Fe^{III}Fe^{III}$...$Cr^{III}L$ state as determined by UV−vis absorbance at 422 nm.

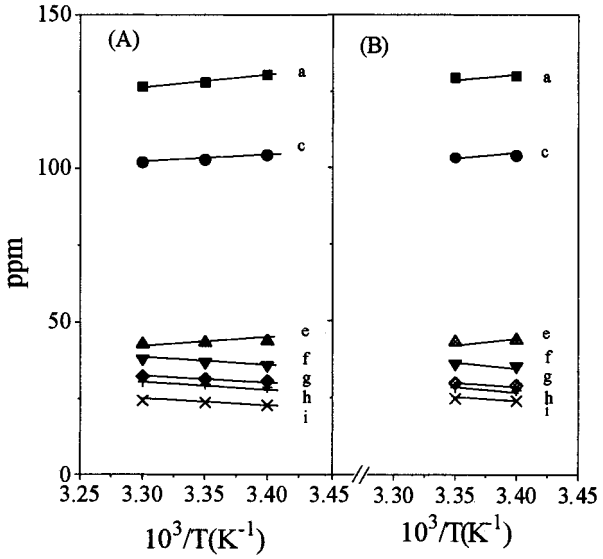

Figure 6. Curie plots for hyperfine shifted resonances of parsley [2Fe-2S] FdI: (A) native $Fe^{II}Fe^{III}$ form and (B) $Fe^{II}Fe^{III}$...$Cr^{III}L$ forms, with the signals labeled as in Figure 5

2D ^{1}H NMR on Parsley Cr-Modified Ferredoxin. The intensity of the NOESY cross peaks obtained in this study are essentially proportional to the cross relaxation, which is proportional to the reciprocal of the sixth power of the distance separating two nuclei and depends on the correlation time (τ_c) for the reorientation of the two spins. The value of τ_c is determined by the rotational correlation time (τ_r), which depends on the size of the molecule, with the detection of cross peaks depending on the signal-to-noise ratio. A large line width (shorter T_2) determines cross peaks of small height, which can be difficult to extract from the noise. The optimization of mixing time is essential for maximum intensity and low signal-to-noise ratio, with the intensity also depending on T_1 values for the two coupled signals. In such a paramagnetic system the line

(42) Aliverti, A.; Hagen, W. R.; Zanetti, G. *FEBS Lett.* **1995**, *368*, 220−224.
(43) Sayle, R. *RASMOL*; Biomolecular Structure Department, Glaxo Research and Development: Greenford, Middlesex, U.K., 1994.
(44) Bertini, I.; Luchinat, C. In *NMR of Paramagnetic Molecules in Biological Systems*; Physical Bioinorganic Chemistry Series, 3; The Benjamin Cummings Publishing Company Inc.: Menlo Park, CA, 1986.
(45) Bertini, I.; Lanini, G.; Luchinat, C. *Inorg. Chem.* **1984**, *23*, 2729−2730.

Table 2. NOESY Cross Peaks with the Largest Broadening (Factor >16) of the Cr-Modified Parsley FdI

region	cross peak
A	Cys18HN-Cys18Hα, Cys18Hα-ProHγ2, Cys18Hα-Val22Hγ2, Asp19HN-Cys18Hβ3, Asp19HN-Val22Hγ1, Asp19Hβ2-Asp22Hγ1, Asp19Hβ3-Asp22Hγ2, Asp19Hβ3-Val22Hγ1, Asp19Hβ3-Val22 HN, Asp21Hα-Val22HN, Asp21HN-Tyr80Hδ, Val22Qγ1-Tyr80Hϵ, Glu29Hα-Glu29HN, Glu29HN-Ala28Hβ, Glu30HN-Ala28Hα, Glu30HN-Ala28Hβ, Glu30Hγ-Gln27Hα, Ile33HN-Ile33Hα,
B	His90Hβ-Thr9Hα, His90Hβ-Thr89Hγ1, His90Hβ−Lys91HN, Lys91Hγ2-Gly49Hα2, Lys91Hα-Glu93HN, Glu92Hα−Ile95Hδ1, Glu94Hγ2-Ile95Hγ2, Ile95Hγ2-Tyr73Hβ2, Ile95Hγ2−Gln68Hβ3, Ile95Hγ2-Va196HN, Ile95HN-Glu94Hβ Phe63Hϵ-Ile95Hγ2, Phe63Hδ-Val96Hγ1

width is largely determined by the paramagnetic contributions of $Cr^{III}L$. Therefore for fast relaxing systems, a short mixing and recycling time must be used in order to avoid complete relaxation of the signals before acquisition, and to increase the number of scans per experiment time. For the Cr-modified protein, $Fe^{III}Fe^{III}...Cr^{III}L$, the same NOESY conditions were used as for determination of the solution structure of native parsley FdI,[16] with the only change the difference in mixing times 40, 100, and 300 ms. Cross-peak intensities of native and Cr-modified FdI were compared, to detect the difference due to paramagnetic contributions from $Cr^{III}L$. Nuclei which are close to the paramagnetic $Cr^{III}L$ have shorter T_1 and T_2 values as compared to the native protein, with a result that peak intensities of nuclei affected become smaller in experiments performed with normal mixing and acquisition times in the two dimensions. The volumes of cross peaks of native and Cr-modified protein were obtained using a manual integration program XEASY.[40] The volume of the two NOESY spectra (native and Cr-modified) were calibrated using average ratios for the least changed peak volumes in both spectra. It should be noted that many cross peaks overlap each other, with some cross peaks containing more than two NOE's. These were excluded to determine more accurately volume ratios.

From a comparison of peak volume ratios of native and Cr-modified proteins a three-step strategy was used to identify amino acids affected by the $Cr^{III}L$. The first step was to identify cross peaks, which had disappeared for Cr-modified protein due to broadening caused by the paramagnetic $Cr^{III}L$ in the NOESY (100 ms) spectra. The second step involved normalizing the intensity of these two spectra, by equating the least changed peak volumes on both native and Cr-modified protein. After normalization, the peak ratio volumes for native and Cr-modified protein were divided in classes as follows: 0.8−1.5, 1.5−8, 8−16, and greater than 16. These numbers indicate no broadening, small broadening, medium broadening, and extensive broadening, respectively. The final step involves determining the distance between the larger broadened cross peaks and those showing no broadening, with the assignment of all inter- and intra-residual connectivities compared with data for native protein.[15]

Cross peaks with large broadening (>16) are shown in Table 2. Residues 38−40, 43−48, 62, and 75−77 were not assigned in the native proteins because of their close proximity to the paramagnetic binuclear iron center. From the ratios close to 1.0 of several of their cross peaks, residues 1−17, 24−26, 28, 31−36, 50−58, 64−68, 70−73, 79−91, and 95 are not involved as $Cr^{III}L$ binding. The following amino acids experienced medium broadening and, together with the residues originating the cross peaks in Table 2, contribute to define possible binding sites for the $Cr^{III}L$: 19−22, 27, 29−30, 59−61, 63, 69, 92−94, and 96. In the case of residue 29, which exhibits Glu29 HN−Glu29Hγ3, a factor of about 1 was found, and this residue can therefore be excluded. Residues 59−61, 63, and 69 are close to the paramagnetic iron center and, therefore, must be considered with caution. Figure 7 shows a section of the NOESY spectrum for

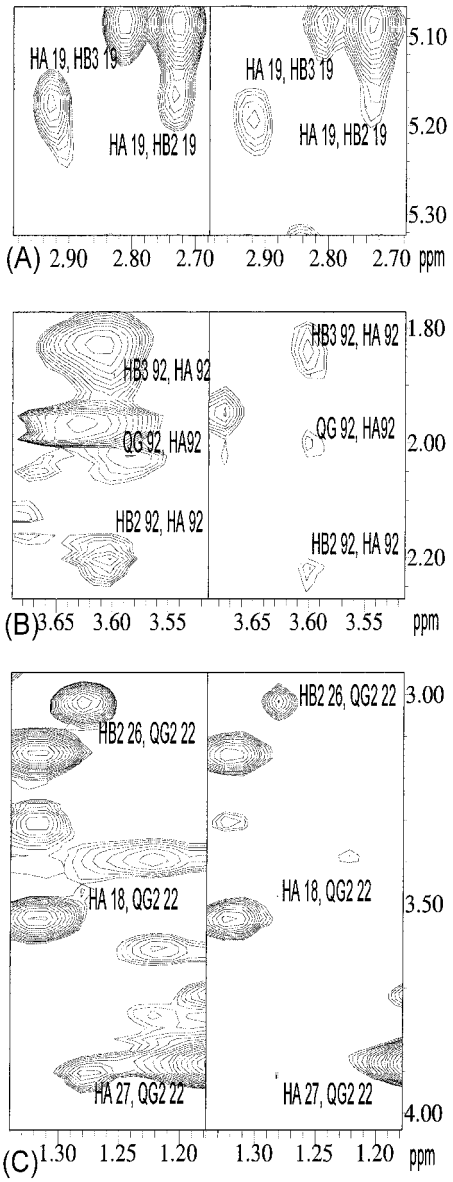

Figure 7. Examples of broadening and/or disappearance of peaks in the 2D NOESY spectrum of the $Cr^{III}L$-modified protein compared to those of the native protein. The left and right parts refer to the native and the $Cr^{III}L$-modified protein, respectively: (A) Asp-19; (B) Glu-92; (C) Val-22.

line broadening of intraresidual cross peaks corresponding to Asp-19, Val-22, and Glu-92.

From these analyses it appears that two distinct regions on the protein surface are affected by the $Cr^{III}L$, Figure 8. Region A (largest broadening, factor >16) consists of the following residues: Asp-19, Asp-20, Asp-21, Val-22, Gln-27, and Glu-30, with Val-22 showing the greatest broadening, and Gln-27 the least. Region A includes Cys-18 which, however, from studies on the native protein, would appear to be solvent

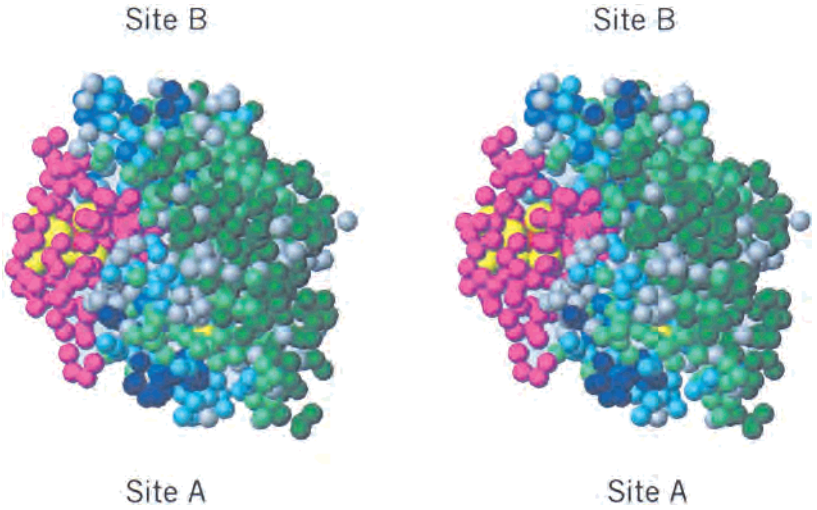

Figure 8. Space-filling proton-only representation of parsley [2Fe-2S] FdI[15] showing the two binding sites, A and B. Color coding is as follows: magenta, not assigned due to Fe_2S_2 cluster proximity (cluster sulfurs in yellow); dark green, peak ratio 0.8−1.5; pale green, peak ratio 1.8−8; sky blue, peak ratio 8−16; royal blue, peak ratios >16; navy, broadened beyond detection.

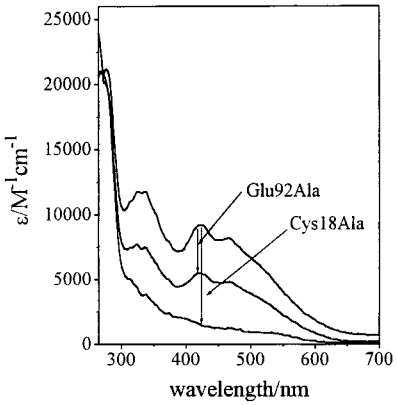

Figure 9. Changes in UV−vis spectra corresponding to the 1 and 2 equiv $Cr^{II}L$ reductions of the Glu92Ala and Cys18Ala spinach Fe^{III}-Fe^{III} variants at pH 7.5 (20 mM Tris/HCl), $I = 0.100$ M (NaCl).

inaccessible with the side chain buried inside the protein.[16] Region B (mostly displaying peak ratios of 8−16) consists of Glu-92, Glu-93, Glu-94, and Val-96. It should be noted that A and B are on opposite sides of the protein, Figure 8.

$Cr^{II}L$ Reduction of Cys18Ala and Glu92Ala Spinach FdI Variants. Spectrophotometric changes for the Cys18Ala variant with a 3-fold excess of $Cr^{II}L$ gave absorbance changes, Figure 9, consistent with a 2-equiv reduction to the $Fe^{II}Fe^{II}$ state (reaction 1). Air oxidation yields the $Fe^{III}Fe^{III}$...$Cr^{III}L$ product

$$Fe^{III}Fe^{III} + Cr^{II}L \rightarrow Fe^{II}Fe^{III}...Cr^{III}L \xrightarrow{+Cr^{II}L} Fe^{II}Fe^{II}...Cr^{III}L + Cr^{III}L \quad (1)$$

(Scheme 1), which was analyzed by ICP-AES and EIMS, Table 1. Different behavior is observed in the case of the Glu92Ala variant, with only 1 equiv reduction to $Fe^{II}Fe^{III}$...$Cr^{III}L$ observed (reaction 2), Figure 9.

$$Fe^{III}Fe^{III} + Cr^{II}L \rightarrow Fe^{II}Fe^{III}...Cr^{III}L \quad (2)$$

Kinetic studies were carried out on the $Cr^{II}L$ reduction of both variants ($Cr^{II}L$ in >10-fold excess). With Cys18Ala, first-order rate constants k_{1obs} and k_{2obs} (25 °C), Table 3, give dependencies on [$Cr^{II}L$], Figure 10. Second-order rate constants from the slopes are $k_1 = 2270 \pm 50$ M^{-1} s^{-1} and $k_2 = 490 \pm 60$ M^{-1} s^{-1} at pH 7.5 (20 mM Tris/HCl), $I = 0.100$ M (NaCl)

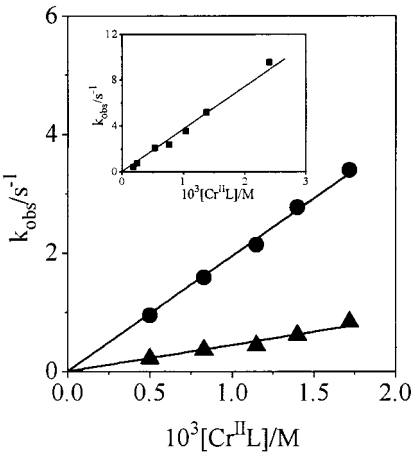

Figure 10. Dependence of rate constants (25 °C) for the reduction of spinach [2Fe-2S] FdI variants (~1×10^{-5} M) with $Cr^{II}L$ (reactant in >10-fold excess). Main plot: the two-stage k_{1obs} (●) and k_{2obs} (▲) reduction of Cys18Ala. Inset: the one-stage (k_{1obs}) reduction of Glu92Ala, at pH 7.5 (20 mM Tris/HCl), $I = 0.100$ M (NaCl).

Table 3. First-Order Rate Constants k_{1obs} and k_{2obs} (25 °C) for the Reduction of the Spinach [2Fe-2S] FdI Variants, Cysl8Ala and Glu92Ala, by the $Cr^{II}L$ Reductant, $[Cr(15\text{-ane}N_4)(H_2O)_2]^{2+}$, at pH 7.5 (20 mM Tris/HCl), $I = 0.100$ M (NaCl)

variant	10^3[$Cr^{II}L$]/M	k_{1obs}/s^{-1}	k_{2obs}/s^{-1}
Cys18Ala	0.50	0.94	0.21
	0.83	1.58	0.36
	1.15	2.13	0.43
	1.40	2.76	0.61
	1.72	3.39	0.83
Glu92Ala	0.19	0.41	
	0.25	0.73	
	0.54	2.07	
	0.77	2.36	
	1.04	3.52	
	1.38	5.13	
	2.40	9.50	

(Table 4). With the Glu92Ala variant, uniphasic kinetics only were detected, giving first-order rate constants k_{1obs}, Table 3. From the dependence on [$Cr^{II}L$], Figure 10, the second-order rate constant is $k_1 = 4060 + 140$ M^{-1} s^{-1}, pH 7.5 (20 mM Tris/HCl), $I = 0.100$ M (NaCl).

Effects of $Cr^{III}L$ Modification on Biological Electron Transfer. The effectiveness of the attached $Cr^{III}L$ of parsley

Table 4. Comparisons of Second-Order Rate Constants (25 °C) for the $Cr^{II}L$ Reduction of Various $Fe^{III}Fe^{III}$ [2Fe-2S] Ferredoxins, pH 7.5, $I = 0.100$ M (NaCl)[a]

[2Fe-2S] FdI	$k_1/M^{-1}\ s^{-1}$	$k_2/M^{-1}\ s^{-1}$
parsley[b]	1510(64)	210(19)
spinach[b]	2760(60)	660(20)
A. variabilis[b]	1250(40)	
spinach Cys18Ala	2270(50)	490(60)
spinach Glu92Ala	4060(140)	

[a] Errors are indicated in parentheses. [b] See ref 24.

$Fe^{III}Fe^{III}$...$Cr^{III}L$ Fd on ET in the NADPH−cytochrome *c* reductase reaction catalyzed by FNR was tested by steady-state kinetics.[29] Whereas the K_M value of FNR for the $Cr^{III}L$-modified Fd was not substantially changed as compared with that for the unmodified Fd, the k_{cat} value using $Cr^{III}L$-modified Fd was increased 2-fold ($193 \pm 4\ s^{-1}$ vs $95 \pm 3\ s^{-1}$).

Discussion

In this paper studies on the reduction of plant [2Fe-2S] Fds with $Cr^{II}L$ have been extended to determine the site on the Fd at which the $Cr^{III}L$ product becomes attached. To achieve this a sample of parsley FdI in the $Fe^{III}Fe^{III}$...$Cr^{III}L$ state, the so-called $Cr^{III}L$-modified form, was prepared as indicated in Scheme 1. Both 1D and 2D ^1H NMR techniques have been used along with assignments provided by the NMR solution structure of parsley $Fe^{III}Fe^{III}$ FdI.[16]

As in the case of parsley and spinach $Fe^{III}Fe^{III}$ FdI, the $Cr^{II}L$ reduction of the FdII forms (which introduce further amino acid variations!) give absorbance changes which are consistent with two-stage reactions to the $Fe^{II}Fe^{II}$ state. Metal analyses on the air-oxidized $Fe^{III}Fe^{III}$...$Cr^{III}L$ products (Scheme 1) confirm the attachment of a single $Cr^{III}L$, Table 1. From known amino acid sequences for spinach FdI, spinach FdII, and parsley FdI, Figure 3, all three have a cysteine at position 18. On the other hand, *A. variabilis*,[24] which does not bind $Cr^{III}L$, has a valine at position 18 and no free cysteine. These observations appear to strengthen further the case for Cys-18 as a site for $Cr^{III}L$ attachment. The spinach Cys18Ala variant was prepared to specifically address this question.

The 1D NMR spectra for native and $Cr^{III}L$-modified FdI show typical behavior on varying the temperature, Figure 5. Both Curie and anti-Curie shifts of α and β proton resonances of the active-site cysteines coordinated to Fe^{II} and Fe^{III}, respectively, are observed, Figure 6. No differences were observed for the $Fe^{III}Fe^{III}$ and one-electron-reduced states in the far downfield region, whereas for the less downfield region a new peak for the $Fe^{II}Fe^{III}$...$Cr^{III}L$ protein was observed at 25 ppm and 288 K. There are four peaks in this less downfield region, which have been assigned to specific protons of the active-site cysteines, and on increasing the temperature the new peak appears to shift downfield to merge with these four peaks. The similarity of the spectra of the $Fe^{II}Fe^{III}$-containing species, with and without $Cr^{III}L$ attached, suggests that the site of $Cr^{III}L$ binding is remote from the four active-site cysteines. This assumption is in keeping with EPR saturation studies which indicate that the $Cr^{III}L$ is ∼15 Å from Fe_B.[24] The two-electron-reduced spectrum of $Fe^{II}Fe^{II}$...$Cr^{III}L$ shows a broad peak at 34.5 ppm, Figure 5, which is the same shape as that observed for native $Fe^{III}Fe^{III}$ (35.4 ppm). Spin coupling of the $Fe^{II}Fe^{II}$ component gives a diamagnetic center as in the case of the Fe^{III}-Fe^{III} protein, and the similar spectra are therefore as expected.

The 2D NOESY spectrum of the $Cr^{III}L$-modified protein has a number of peaks with large broadening as compared to the native NOESY spectrum. The residues with the largest broadening factor, due to the close proximity of the paramagnetic $Cr^{III}L$ complex, are 19−22, 27, 30, 92−94, and 96. These residues occur in two regions of the protein, Figure 1. Site A consists of residues 19−22, 27, and 30. The residues here are mainly acidic (Asp-19, Asp-20, Asp-21, Val-22, Gln-27, and Glu-30), and Cys-18 is also in this region. Site B consists of Glu-92−94 and Val-96. Figure 8 shows the position of A and B on opposite sides of the protein. Site A gives the larger broadening effects with many peaks giving ratios >16 (very large broadening), which suggests this as the site of $Cr^{III}L$ binding. A number of acidic residues are broadened by the $Cr^{III}L$. The residue showing the largest broadening is Val-22, with four nearby acidic residues Asp-19, Asp-20, Asp-21, and Glu-30 the next most broadened. An explanation in terms of attachment of $Cr^{III}L$ at one or more of the carboxylates close to Val-22 (which cannot itself bind $Cr^{III}L$) is likely. The Gln-27 residue is less broadened.

The NMR studies also indicate that site B is affected by $Cr^{III}L$, but the broadening is less extensive than at A. As with A the region includes conserved acidic residues, Glu-92−94. The broadening around B suggests that a second $Cr^{III}L$ is bound, but this is not possible from ICP-AES and EIMS analyses, Table 1. This leads to a consideration of protein association in the NMR experiments, since 3−4 mM concentrations of the $Cr^{III}L$-modified protein give solutions which are quite compact in terms of protein. As a result two Cr-modified protein molecules might associate in a head to tail fashion so that all A sites have a $Cr^{III}L$ attached, and 50% of B sites interact with a bound $Cr^{III}L$, Figure 11. If three protein molecules associate, then all A sites will have a $Cr^{III}L$ attached and 66% of B sites will interact with a bound $Cr^{III}L$, Figure 11. It should be recalled that in the case of spinach FdI the crystal packing of the Glu92Lys variant reveals that Lys-92 is H-bonded to Asp-26 of a symmetry-related molecule.[12] These two residues are in the same surface regions (A and B) of ferredoxin proposed here to be linked through $Cr^{III}L$.

Site A includes Cys-18, which has been considered as a possible residue for $Cr^{III}L$ attachment.[24] However, from the NMR solution structure of parsley FdI,[16] Cys-18 is not solvent accessible, and the thiolate group is buried within the protein. No broadening of Cys-18 is observed in the case of the Fe^{III}-Fe^{III}...$Cr^{III}L$ protein, and Cys-18 is unlikely therefore to be the binding site for $Cr^{III}L$. This is confirmed by studies on the $Cr^{II}L$ reduction of the spinach FdI Cys18Ala variant, when 1 mol of $Cr^{III}L$ still becomes attached to the protein and two-electron reduction to $Fe^{II}Fe^{II}$ occurs, Table 1. The reduction potential of the variant is practically unchanged at −450 mV vs NHE. Since rate constants k_1 and k_2 are similar to those for native spinach, Table 4, similar processes are implied.

The spinach Glu92Ala variant was used to test the ET reactivity of site B. Acidic residues at (or near to) this site have been found to be important in redox reactions of *Anabaena* 7120[46,47] and spinach FdI[29,42] with the physiological partner FNR, and the Glu-92 residue received particular mention. On reduction of spinach Glu92Ala with excess $Cr^{II}L$ the $Fe^{III}Fe^{III}$ form gives monophasic absorbance changes (Table 3), and the $Fe^{II}Fe^{III}$ state is the final product with a single $Cr^{III}L$ attached.

(46) Hurley, J. K.; Weber-Main, A. M.; Stankovich, M. T.; Benning, M. M.; Thoden, J. B.; Van-Hooke, J. L.; Holden, H. M.; Chae, Y. K.; Xia, B.; Cheng, H.; Markley, J. L.; Martinez-Julves, M.; Gomez-Moreno, C.; Schemetis, J. L.; Tollin, G. *Biochemistry* **1997**, *36*, 11100−11117.

(47) Holden, H. M.; Jacobsen, B. L.; Hurley, J. K.; Tollin, G.; Oh, B.-H.; Skjedal, L.; Chae, Y. K.; Xia, B.; Markley, J. L. *J. Bioenerg. Biomembr*. **1994**, *26*, 67−68.

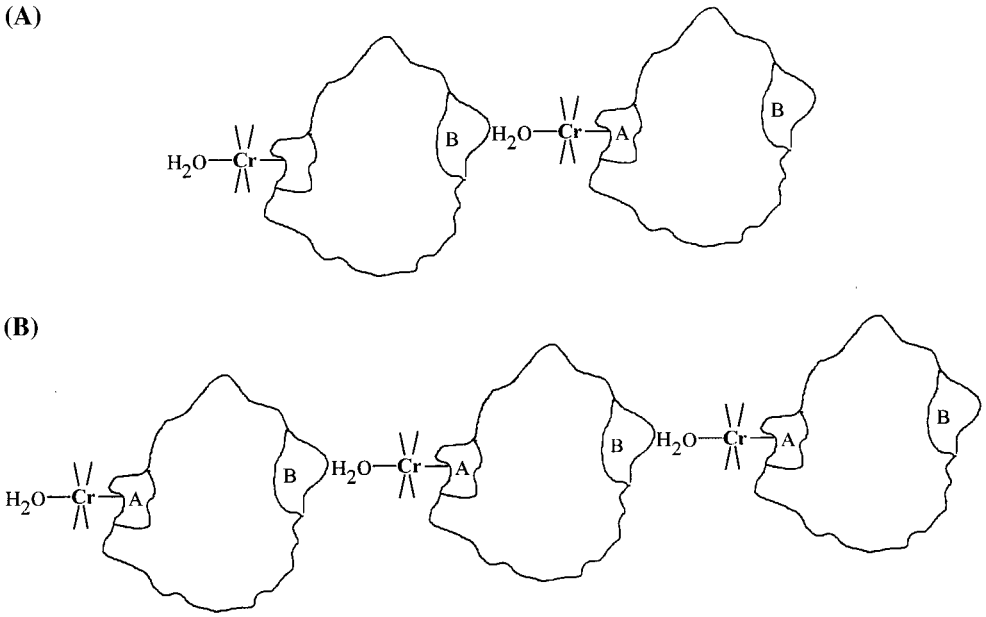

Figure 11. The intermolecular electrostatic association of $Fe^{III}Fe^{III}$...$Cr^{III}L$ protein molecules to give (A) dimer and (B) trimer forms as an explanation of $Cr^{III}L$ NMR line-broadening effects at the two sites A and B on each molecule.

The second-order rate constant is similar to that obtained for the first stage (k_1) of reaction of the Fe^{III} Fe^{III} native protein (~2-fold increase), Table 4. The Glu92Ala variant therefore exhibits novel behavior, with attachment of $Cr^{III}L$ as observed for parsley and spinach FdI and FdII, but no second-stage reduction to $Fe^{II}Fe^{II}$. This is surprising because not only does the Glu92Ala have a more positive reduction potential of −342 mV vs NHE but, on attachment of $Cr^{III}L$, the reduction potential has been observed to be a further ~200 mV more positive.[24] The first effect has been attributed to H-bonding of Glu-92[46,48] to Ser-45 and hence to the active site Cys-44 bonded to Fe_A.[49] Removal of Glu-92 not only disrupts the H-bonding but eliminates what appears to be a highly specific pathway for ET. It is concluded that Glu-92 is a candidate as site of reduction by the second $Cr^{II}L$, when $Cr^{III}L$ attached at A has the effect of making the driving force more favorable.

The exact site of $Cr^{III}L$ attachment at A is not established, but four acidic residues Asp-19, Asp-20, Asp-21, and Glu-30 are identified as candidates. Of these Asp-19 can be excluded because it is replaced by Pro in spinach FdI. A carboxylate residue which is not H-bonded can be seen as a more likely site for inner-sphere reduction by $Cr^{II}L$ than one that is H-bonded. From the NMR solution structure of parsley FdI,[16] and similar information from the *Anabaena* 7120 X-ray crystal structure,[8] information has been obtained regarding the extent of H-bonding using the program MOL-MOL with distance and angle constraints set at <2.50 Å and 120.0°, respectively.[50] It is apparent that, for parsley, residues 16−31 (some of which are components of site A) show most difference in H-bonding. Two residues at A, Asp-21 and Gln-27, which are broadened in the studies on parsley FdI are not involved in H-bonding. Of these Asp-21 has the larger broadening and next to Val-22 produces the largest effect. Solvent accessibility data indicate that, of all the residues undergoing broadening in this region, Asp-21 is the most exposed (48.0%). Thus for parsley FdI Asp-21 may be regarded as the most favorable site for $Cr^{III}L$ attachment. The corresponding two acidic residues in *Anabaena* 7120 are H-bonded, so that when $Cr^{II}L$ is used as a reductant for *A. variabilis* $Fe^{III}Fe^{III}$ FdI the $Cr^{III}L$ is not bound to the protein. H-bonding is therefore able to explain the different behavior of parsley and spinach Fd forms as opposed to *A. variabilis* FdI.

When $Cr^{II}L$ is the reductant at site A, the reaction occurs by an inner-sphere mechanism (with bonding to the protein), and $Cr^{III}L$ remains attached to the product. The second stage of reaction, which is more favorable with $Cr^{III}L$ attached at A, then occurs at Glu-92 of site B. This is, however, an outer-sphere process since the second Cr^{III} L does not become attached to the protein. The reaction of $Cr^{II}L$ at A is some seven times more favorable than at B for parsley and spinach FdI. From structure coordinates,[16] the direct distance of a number of acidic residues at A to the nearest point of the $Fe_2S_2(Cys)_4$ active site can be measured. Of these the distance from the carboxylate O atom of Asp-21 to the S atom of Cys-77 is ~18 Å. The distance is greater than the corresponding distance of Glu-92 at B to the S atom of Cys-44, which is ~11 Å. Because of the H-bonding at site B (see above), the reaction of $Cr^{II}L$ is outer-sphere, and no $Cr^{III}L$ attachment occurs. In addition the most favorable pathway for ET from Glu-92 to Cys-44 involves two H-bonds, which are generally regarded as less favorable, and the reaction is slower.[51,52] No ET from B appears to be observed on replacement of Glu-92 with Ala, suggesting that Glu-92 is important as a lead-in group.

The charge balance on the ferredoxins at −18(±2) is unusually high, and the attachment of 3+ $Cr^{III}L$ to the surface has a large and controlling influence on reactivity. Thus the $E^{\circ\prime}$ for the native spinach $Fe^{III}_2/Fe^{II}Fe^{III}$ couple −462 mV vs NHE decreases to −273 mV vs NHE on attachment of $Cr^{III}L$,[24] and for the second-electron reduction an $E^{\circ\prime}$ of −410 mV vs NHE has been determined.[24] To a lesser degree the same may be true on attachment of the $Cr^{II}L$ reductant, which may be an

(48) Vidakovic, M.; Fraczkiewicz, G.; Dave, B. C.; Czernuszewicz, R. S.; Germanas, J. P. *Biochemistry* **1995**, *34*, 13906−13913.
(49) Taylor, R.; Kennard, O.; Verichel, W. *J. Am. Chem. Soc*. **1983**, *105*, 5761−5766.
(50) Beratan, D. N.; Onuchic, J. N. *Photosynth. Res*. **1989**, *22*, 173−186.
(51) Beratan, D. N.; Onuchic, J. N.; Betts, J. N.; Bowler, B. E.; Gray, H. B. *J. Am. Chem. Soc*. **1990**, *112*, 7915−7921.
(52) Zanetti, G.; Morelli, D.; Ronchi, S.; Negri, A.; Aliverti, A.; Curti, B. *Biochemistry* **1988**, *27*, 3753−3759.

important factor in favoring the inner-sphere reaction at A. Interestingly, there is no apparent effect of $Cr^{III}L$ modification of Fd on its interaction with FNR. Thus, binding of $Cr^{III}L$ to site A does not perturb the protein−protein interaction. This is in keeping with the model of the Fd−FNR complex proposed on the basis of cross-linking studies,[52] and homology observed with phthalate dioxygenase reductase.[53]

Conclusion

To summarize, using 1D and 2D ^1H NMR methods, residues 19−22, 27, and 30 at site A have been identified as candidates for the binding of the reductant $Cr^{II}L$ as $Cr^{III}L$ to parsley Fe^{III}-Fe^{III} FdI. Similar binding is observed for parsley FdII and for spinach FdI and FdII. Studies on the spinach Cys18Ala variant have confirmed that the Cys-18 at A is not involved in the binding, and on present evidence the carboxylate of Asp-21 is the likely point of attachment. This implies a distance for ET of ∼18 Å from the Cr^{II} to the S(Cys-77) at the active site. At 3−4 mM levels of $Fe^{III}Fe^{III}$...$Cr^{III}L$ used in the NMR experiments, the single $Cr^{III}L$ attached at A interacts at site B (residues 92−94 and 96) on a second molecule. Site B is on the opposite side of the molecule from A, and such association gives rise to less strong $Cr^{III}L$ line broadening at site B. Since no second stage is observed with the Glu92Ala variant, Glu-92 at site B is established as the most likely point for the second slower stage of $Cr^{II}L$ reduction of the $Fe^{II}Fe^{III}$...$Cr^{III}L$ intermediate to $Fe^{II}Fe^{II}$...$Cr^{III}L$. The relative effectiveness of A and B as sites for inner-sphere (site A) and outer-sphere (site B) ET reaction is thus established. To summarize, attachment of the +3 $Cr^{III}L$ complex to the −18 charged protein (97 amino acids) at A has a large effect (∼200 mV) on the reduction potential, making further $Cr^{II}L$ reduction of $Fe^{II}Fe^{III}$...$Cr^{III}L$ to $Fe^{II}Fe^{II}$...$Cr^{III}L$ possible at B.

Acknowledgment. Financial support from the UK Engineering and Physical Sciences Research Council are gratefully acknowledged (J.A.R.W. and S.-C.I.), as well as Consiglio Nazionale delle Ricerche of Italy (G.Z.). The NMR data were collected at the Florence Large Scale Facility PARABIO (ERBFMGECT950033 (DG12)), and the visit of A.G.S. and J.A.R.W. to the facilities was also supported by the EU.

IC991127W

(53) Correl, C. C.; Ludwig, M.; Bruns, C. M.; Karplus, P. A. *Protein Sci.* **1993**, *2*, 2112−2133.